Article

Dissolved Organic Matter Photoreactivity Is Determined by Its Optical Properties, Redox Activity, and Molecular Composition

Stephanie M. Berg, Kristine H. Wammer, and Christina K. Remucal*

Cite This: Environ. Sci. Technol. 2023, 57, 6703−6711

Read Online

ACCESS | Metrics & More | Article Recommendations | Supporting Information

ABSTRACT: Predicting the formation of photochemically produced reactive intermediates (PPRI) during the irradiation of dissolved organic matter (DOM) has remained challenging given the complex nature of this material and differences in PPRI formation mechanisms. We investigate the role of DOM composition in photoreactivity using 48 samples that span the range of DOM in freshwater systems and wastewater. We relate quantum yields for excited triplet-state organic matter (f_{TMP}), singlet oxygen ($\Phi_{^1O_2}$), and hydroxylating species ($\Phi_{\bullet OH}$) to DOM composition determined using spectroscopy, Fourier-transform ion cyclotron resonance mass spectrometry, and electron-donating capacity (EDC). f_{TMP} and $\Phi_{^1O_2}$ follow similar trends and are correlated with bulk properties derived from UV−vis spectra and EDC. In contrast, no individual bulk property can be used to predict $\Phi_{\bullet OH}$. At the molecular level, the subset of DOM that is positively correlated to both $\Phi_{\bullet OH}$ and EDC is distinct from DOM formulas related to $\Phi_{^1O_2}$, demonstrating that $\bullet OH$ and $^1O_2$ are formed from different DOM fractions. Multiple linear regressions are used to relate quantum yields of each PPRI to DOM composition parameters derived from multiple techniques, demonstrating that complementary methods are ideal for characterizing DOM because each technique only samples a subset of DOM.

Predicting photoreactivity of 48 diverse waters

Key DOM Analyses		^{3}DOM	$^1O_2$	$\bullet$OH
UV-vis	E_2:E_3	+++	++	
Fluorescence	HIX	++		
	FI		+++	++
Electron donating capacity	EDC	− − −	− − −	
Molecular composition	H:C_w			
	O:C_w			− −

KEYWORDS: photoreactivity, indirect photolysis, dissolved organic matter, high-resolution mass spectrometry

INTRODUCTION

Dissolved organic matter (DOM) is a complex mixture of organic molecules derived from terrestrial and microbial sources.[1,2] Environmental processing of DOM further changes its molecular composition and reactivity.[3,4] DOM participates in reactions that affect microbial metabolism,[5] contaminant transformation,[6−8] and drinking water treatment processes.[9−11] In surface waters, DOM is the predominant light absorbing component and forms photochemically produced reactive intermediates (PPRI) as a result.[12,13]

Upon absorption of light, DOM enters its singlet excited state (^{1}DOM), which may undergo intersystem crossing to form the longer-lived triplet excited state (^{3}DOM).[13] The predominant quencher of ^{3}DOM is O_2, which forms singlet oxygen ($^1O_2$) via energy transfer from ^{3}DOM. Both ^{3}DOM and $^1O_2$ can react to transform some organic contaminants.[7,14,15] Autochthonous DOM or DOM originating from wastewater has been shown to be more photoreactive in terms of producing these PPRI.[14,16,17] Other PPRI, including hydrogen peroxide (H_2O_2), superoxide, ($O_2^{\bullet-}$), and hydroxyl radical ($\bullet OH$), form through electron-transfer reactions, but exact pathways are less well understood.[18,19] The two predominant mechanisms discussed in the literature include reduction of O_2 or H-atom abstraction from water.[20] Precursors for these PPRI may include ^{1}DOM, ^{3}DOM, charge-transfer species, or other photochemically excited complexes associated with DOM.[21−23]

Conflicting evidence exists about relationships between ^{3}DOM quantum yield coefficients (f_{TMP}) and $^1O_2$ quantum yields ($\Phi_{^1O_2}$) as compared to those for $\Phi_{\bullet OH}$, which is likely because ^{3}DOM and $^1O_2$ form via energy transfer and $\bullet OH$ results from electron transfer.[14,22,24] For example, f_{TMP} and $\Phi_{^1O_2}$ are often correlated with each other and with properties derived from UV−vis spectroscopy, such as E_2:E_3 (i.e., the ratio of absorbance at 250 to 365 nm).[16,25−30] In contrast, $\Phi_{\bullet OH}$ has the same trends as other PPRI or E_2:E_3 in some studies[24,31,32] but opposite trends in other studies.[17,33−35] ^{3}DOM and $^1O_2$ quantum yields are positively correlated with

the same pools of highly aliphatic DOM at the molecular level in several small sets of samples,[14,26,36] and we previously demonstrated that separate pools of DOM are strongly related to f_{TMP} and $\Phi_{^1O_2}$ in comparison with $\Phi_{•OH}$.[14] However, these molecular level trends have not yet been tested in diverse waters.

Measures of redox activity have also been related to photochemical reactivity in a small number of studies. For example, antioxidant capacity measurements via reaction of DOM with 2,2-diphenyl-1-picrylhydrazyl are negatively correlated to f_{TMP} and $\Phi_{^1O_2}$.[31] Electron-donating capacity (EDC) measured via cyclic voltammetry is unrelated to $\Phi_{^1O_2}$ but positively correlated to quantum yields for H_2O_2 formation.[30] Redox activities of DOM have been correlated with absorbance and fluorescence data in photochemical studies but have not yet been related to molecular composition data such as that acquired via ultrahigh-resolution mass spectrometry. Because $•OH$ is formed via electron transfer, EDC measurements may prove useful in predicting formation of this important PPRI.

Because predicting $•OH$ formation has remained elusive in the literature,[31,37] we aim to improve our understanding of PPRI formation by presenting a complete picture of DOM optical properties, redox properties via EDC measurements, molecular composition via high-resolution mass spectrometry, and photochemical reactivity in terms of ^3DOM, $^1O_2$, and $•OH$ formation. We include a large number of samples that span the range of the DOM composition encountered in freshwater systems, including terrestrially derived bogs, microbially derived and altered DOM from oligotrophic lakes, and wastewater and wastewater-impacted samples, to investigate whether previously observed molecular trends[14] are universally true. The unique data set presented here represents the first large-scale assessment of both DOM composition and photoreactivity in diverse freshwaters and includes the first comparison of EDC with DOM molecular composition. Finally, we consider simple linear and multiple linear regression (MLR) models to investigate how DOM properties affect PPRI formation.

■ MATERIALS AND METHODS

Sample Collection. Samples were collected from five geographical locations in Wisconsin and Minnesota, USA between August 2018 and September 2020. Samples include lakes of diverse trophic status ($n = 13$), rivers ($n = 20$), and agricultural ditches ($n = 2$). Additionally, 13 wastewater effluent samples were collected from four wastewater treatment plants (WWTPs). More information about sample sites and collection can be found in Section S1. Chemical sources are described in Section S2.

Water Chemistry Analysis. Chloride, nitrate, nitrite, and sulfate concentrations were measured using ion chromatography. Dissolved organic carbon ([DOC]) and inorganic carbon ([DIC]) concentrations were measured using a Shimadzu total organic carbon analyzer. Calcium, iron, potassium, magnesium, and sodium concentrations were measured using inductively coupled plasma-optical emission spectroscopy. More information on analytical methods is provided in Section S3.

The bulk DOM composition was evaluated in whole water samples using absorbance measurements collected via a HORIBA Aqualog Fluorimeter (Section S3). Parameters including specific absorbance at 254 nm ($SUVA_{254}$) and

E_2:E_3 were calculated as described previously.[38,39] These parameters were corrected for nitrate absorbance, which resulted in changes of ~2%. $SUVA_{254}$ and E_2:E_3 are related to the measurements of aromaticity and molecular weight, respectively.[38–40] Humification index (HIX) and fluorescence index (FI) were also calculated due to their ease of measurement and minimal dependence on inner filtering effects.[41,42] HIX was calculated as the sum of the emission from 435–480 nm divided by the sums of the emission from 300–345 and 435–480 nm with excitation at 254 nm. FI was calculated as the ratio of emission intensities at 470 and 520 nm upon excitation at 370 nm.[42]

The DOM molecular composition was evaluated using Fourier transform-ion cyclotron resonance mass spectrometry (FT-ICR MS). Prior to analysis, DOM was extracted using solid-phase extraction and re-diluted in methanol.[43] Aliquots were diluted in 50:50 acetonitrile/ultrapure water and directly injected into a Bruker FT-ICR MS (Solarix XR 12T) via negative mode electrospray ionization. Exported m/z ions were linearly calibrated and compared with potential formulas containing combinations of $^{13}C_{0–1}{}^{12}C_{5–80}H_{0–120}O_{0–80}N_{0–3}S_{0–1}$ atoms. Matches were verified using a 0.2 ppm mass error cutoff and homologous series requirement as described previously.[14,44] Further information can be found in Section S4. Weighted averages of hydrogen to carbon ratio ($H:C_w$), oxygen to carbon ratio ($O:C_w$), and double bond equivalents (DBE_w) were calculated for each sample.

EDC was measured in whole water samples using the 2,2′-azino-*bis*(3-ethylbenzothiazoline-6-sulfonate) radical cation ($ABTS^{•+}$) as described previously.[45] Briefly, 125 μM $ABTS^{•+}$ was added to each sample (four dilutions per site). The reduction $ABTS^{•+}$ to ABTS by DOM was quantified by loss of absorbance at 728 nm after 15 min of the reaction. EDC was calculated from the difference in $ABTS^{•+}$ between DOM samples and ultrapure water samples (Section S5).

Photochemical Reactivity. Steady-state concentrations and quantum yields of $^1O_2$ and $•OH$ in air-saturated solutions were quantified during irradiation in a Rayonet photoreactor with sixteen 365 nm bulbs (full width half max = ±10 nm).[46] Quantum yield coefficients for ^3DOM (f_{TMP}) were quantified with the same light source with [DOC] diluted to 5 mg-C L^{-1} due to the quenching effect of DOM on the radical cation intermediate of 2,4,6-trimethylphenol (TMP).[26,36,47] Probe compounds (10 μM) furfuryl alcohol (FFA), terephthalic acid (TPA), and TMP were used in separate experiments to measure $^1O_2$, $•OH$, and ^3DOM, respectively, in whole waters.[14,24,48–50] TPA captures both free $•OH$ and other hydroxylating species;[20] we refer to the combination as $•OH$ for simplicity. Triplicate measurements were taken alongside a *p*-nitroanisole/pyridine actinometer to quantify light intensity.[51] Buffer was not added due to precipitation during some irradiations; the pH remained within 0.3 units during experiments. The degradation of FFA and TMP and the formation of the TPA hydroxylation product (i.e., hydroxyterephthalic acid) were measured with high-performance liquid chromatography (Section S6).

Statistical Analyses. In box-and-whisker plots, whiskers represent the first and fourth quartile, the box height represents the second and third quartile, and the horizontal line represents the median; outliers are denoted as individual points. Statistical significance between categorical groups was calculated by ANOVA-Tukey tests. Error bars in all other figures represent one standard deviation of ≥3 replicates.

Spearman rank correlations were calculated by relating the relative formula intensity of individual formulas to another measurement made for that sample (Section S8).[52,53] Only formulas identified in at least three samples were included.

MLR models were constructed for quantum yields using pH, anions, cations, [DIC], $SUVA_{254}$, E_2:E_3, HIX, FI, EDC, H:C_w, and O:C_w as potential predictor variables. These parameters were considered because both DOM composition and water chemistry can affect the photochemical reactivity.[35,54,55] Extrinsic properties in the f_{TMP} MLR were divided by the dilution factors used during photolysis experiments. Models were reduced using Bayesian information criterion with backward stepwise regression. Variation inflation scores meet model assumption about collinearity (i.e., <1.5). A p-value <0.05 was considered to be significant in MLRs and simple linear regressions.

■ RESULTS AND DISCUSSION

Water Chemistry. The 48 samples span the range of DOM types in freshwater systems (Table S1) and vary widely in water chemistry (Figures S1−S11; Tables S2−S4). Natural water samples are categorized into five groups (e.g., St. Louis River (SLR), Northern Lakes, Yahara, Mankato, or Twin Cities) based on their geographical location because land cover influences DOM composition.[56] Wastewater effluents are grouped separately. Elevated ion concentrations are observed in wastewater samples compared to natural waters. High nitrate concentrations in the Mankato and some of the Yahara samples are attributable to agricultural land cover in these areas. High nitrate concentrations are also observed in some wastewater samples (Figure S5; Table S3). Iron, which can participate in photochemical reactions,[57] is observed primarily in the SLR sites (Figure S8; Table S4).

DOC concentrations range from 1.8 to 69 mg-C L^{-1}. The highest [DOC] values are observed in waters with large terrestrial carbon inputs (e.g., SLR samples), and the lowest values are observed in oligotrophic lakes (Figures 1a and S1; Table S2). [DOC] ranges widely in wastewater samples, with high [DOC] in a WWTP that receives significant industrial inputs (53 mg-C L^{-1}; Figure 1).[14,58] Inorganic carbon concentrations range from 1.42 to 92.7 mg-C L^{-1}, with lower concentrations observed in SLR and Northern Lake samples due to underlying geology (Figures S2, S3; Table S2).

DOM Composition. Optical properties derived from UV−vis and fluorescence spectroscopies are used to assess the bulk DOM composition (Figures 1; S12−S17; Table S5). High $SUVA_{254}$ and low E_2:E_3 values are indicative of large, aromatic DOM, while low $SUVA_{254}$ and high E_2;E_3 values are associated with smaller, aliphatic molecules.[38,39] High $SUVA_{254}$ values in SLR samples arise from terrestrially derived DOM upstream in the river.[14] $SUVA_{254}$ values range widely in the Northern Lakes because these lakes include dystrophic bogs and oligotrophic lakes (Figure S13).[16] Samples collected in the Twin Cities have high E_2:E_3 due to three clear lake samples (e.g., Lake Vadnais, Lake Phalen, and Lake of the Isles; Figure 1b). Although low $SUVA_{254}$ and high E_2:E_3 values are expected in wastewater effluent,[58,59] the wastewater-derived samples have optical properties near the middle of ranges observed in this study (Figures S12−S17). Fluorescence indices such as the HIX and FI are associated with terrestrially derived DOM and microbially derived DOM, respectively.[60] The Northern Lakes have a large range in HIX with values in bogs > lakes (Figures
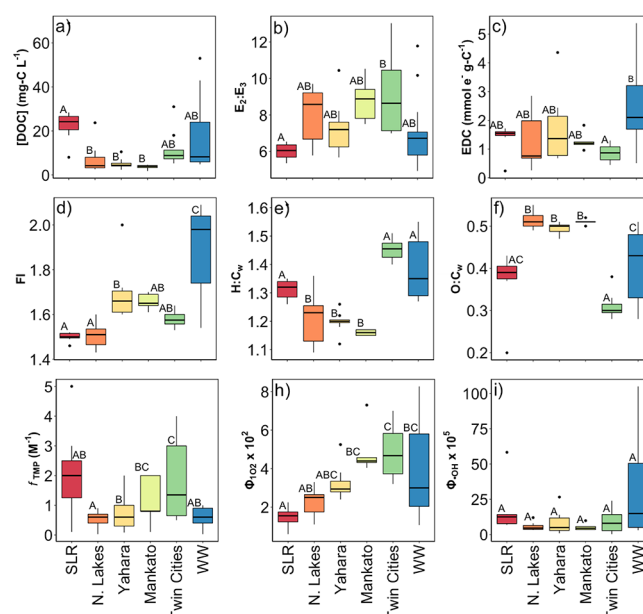

Figure 1. Box and whisker plots grouped by geographical location for (a) DOC concentration, (b) E_2:E_3, (c) EDC, (d) FI, (e) H:C_w, (f) O:C_w, (g) f_{TMP}, (h) $\Phi_{^1O_2}$, and (i) $\Phi_{\bullet OH}$. Statistical significance between categorical groups was calculated by ANOVA-Tukey tests.

S15, S16). FI values show the largest range in the wastewater samples (Figures 1d; S17).

DOM is characterized at the molecular level via FT-ICR MS. A total of 14,318 unique formulas are identified with an average of 4,026 formulas per sample (Table S6). Samples with large amounts of terrestrial input (i.e., SLR and Northern Lakes) are dominated by CHO-only formulas, while wastewater, Yahara, and Mankato samples contain high percentages of nitrogen- and sulfur-containing formulas (Tables S6, S7). H:C_w is higher in wastewater and urban samples compared to that in rural or agriculture samples (Figure 1e), corresponding to more aliphatic DOM. O:C_w is lower in urban samples than that in other groups (Figure 1f), corresponding to more reduced DOM.

To compare the DOM molecular composition from different land cover types, formulas identified in each geographical region are plotted on van Krevelen diagrams (Figure 2). Northern Lake samples have the most unique formulas, especially at high H:C. Formulas only found in the Yahara and Mankato samples are concentrated at low H:C ratios. While the origin of these formulas is unclear, they may be attributable to farmland as both regions are heavily impacted by agriculture. The Twin City samples show unique formulas at low O:C ratios (Figure 2e). Observations of DOM from urban runoff having low O:C have been made previously.[61] Unique wastewater formulas are concentrated in the lipid- and protein-like regions, as observed previously for other wastewater effluents.[14,58,59] The variability in the 48 samples at both the bulk and molecular levels is ideal for assessing how DOM composition impacts its photoreactivity.

Electron-Donating Capacity. EDC is a direct measurement of redox activity and potentially linked to the photoreactivity of DOM, yet is infrequently reported and has not yet been compared with the DOM molecular composition. EDC values range 0.26−5.38 mmol e⁻ g-C^{-1} (Table S5), which agree with previous measurements using the same
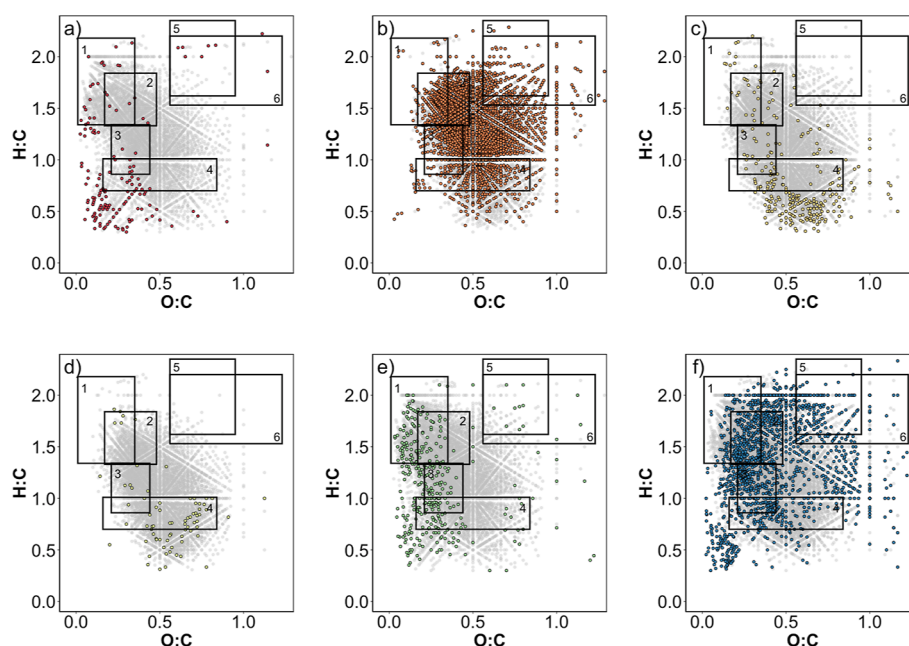
Figure 2. Formulas identified in each of the geographical groups in (a) SLR ($n = 3322$), (b) Northern Lakes ($n = 3521$), (c) Yahara ($n = 5510$), (d) Mankato ($n = 4063$), (e) Twin Cities ($n = 4540$), and (f) wastewater samples ($n = 5663$). Formulas were required to be identified in at least three samples to be considered. Gray points indicate any formula identified in the region. Colored points represent formulas unique to that geographical region. Regions on the plots[83] are designated as (1) lipid-, (2) peptide-, (3) lignin-, (4) tannin-, and (5) carbohydrate-like formulas.
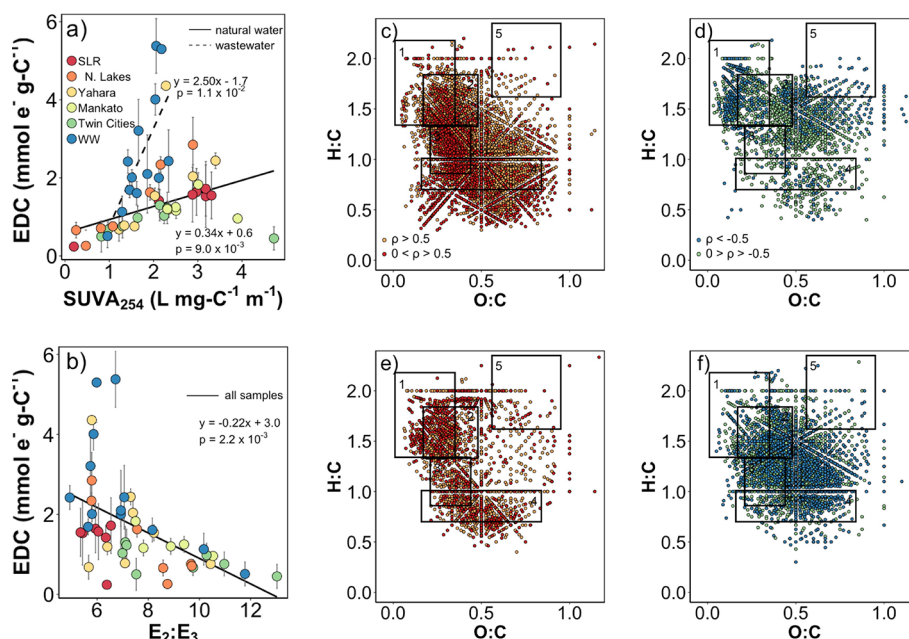

Figure 3. EDC versus (a) $SUVA_{254}$ and (b) $E_2:E_3$. Formulas (c) positively and (d) negatively related to EDC in natural waters. Formulas (e) positively and (f) negatively related to EDC in wastewater. Regions on the plots[83] (c−f) are designated as (1) lipid-, (2) peptide-, (3) lignin-, (4) tannin-, and (5) carbohydrate-like formulas. Absolute Spearmen rho (ρ) values > 0.5 indicate strong correlations. 7,632 formulas were considered for the natural water samples, and 6,553 formulas were considered for the wastewater samples. Formulas were required to be identified in at least three samples to be considered.

spectrophotometric method.[11,45] Terrestrial samples (e.g., bogs and upstream SLR) have higher EDC values than more microbial and/or processed samples (e.g., oligotrophic lakes). Wastewater EDC is highly variable, with values spanning the range observed in the natural waters (0.51−5.38 mmol e⁻ mg-C⁻¹; Figure 1c; Table S5). EDC generally decreases after disinfection with either chlorine or UV in the studied WWTPs,

in agreement with observations using both chlorine[62,63] and ozone[11,45,63] as disinfectants.

EDC is positively correlated with $SUVA_{254}$ and negatively correlated with $E_2:E_3$. The slope for EDC versus $SUVA_{254}$ is similar for all natural water types regardless of land cover or composition of DOM ($p = 0.021$; Figure 3a), in agreement with positive relationships between EDC and measurements of aromaticity via UV−vis[64] and ¹³C NMR.[65] However, the slope

for wastewater samples is much steeper than that of natural water samples (Figure 3a). Different slopes have been documented for EDC between terrestrial and aquatic samples[65] but not specifically for wastewater samples. EDC is negatively related to $E_2{:}E_3$ for the entire data set with some wastewater samples having high EDC ($p = 2.2 \times 10^{-4}$; Figure 3b). EDC is not correlated to HIX ($p = 0.70$; Figure S19a) but is positively correlated to FI ($p = 0.01$; Figure S19b).

EDC is also related to DOM at the molecular level. For natural waters, most lignin- and tannin-like formulas are positively related to EDC (Figure 3c), while saturated formulas show negative relationships (Figure 3d). This result is consistent with the understanding that polyphenolic-like structures give rise to DOM redox activity and agrees with similar analysis comparing $SUVA_{254}$ with the DOM molecular composition.[14,16] In contrast, $H{:}C_w$ is not as strongly related to EDC in wastewater (Figures 3e,f and S20).

While EDC is closely related to the DOM composition in natural water samples, the weaker relationships observed in wastewater samples provide evidence that other structures or interferences within wastewater impact EDC. Given the relatively narrow range in $SUVA_{254}$, the large range in EDC in wastewater samples is unexpected (Figure 3a). Furthermore, we observe that large differences in EDC in wastewater are not attributable to discernible classes of molecular formulas (Figure 3e,f). Studies of DOM redox activity have concluded that phenol and quinone structures are the predominant, but not only, redox active groups within DOM.[23,65−69] In fact, cyclic voltammetry experiments have shown that there is some irreversible redox activity that cannot be attributed to phenols and quinones.[68,70] Heteroatom-containing functional groups likely contribute to overall redox activity[69,71] and are generally enriched in wastewater effluent (Table S7). While other interferences (e.g., reduced forms of metals and ions) may be a confounding factor in EDC measurements, concentrations of these species are low in our samples (Tables S3, S4) and have been ruled negligible in another study considering EDC of wastewater.[45] Collectively, these results demonstrate that EDC is consistently related to multiple bulk and molecular level measurements of DOM composition in surface water samples but that these trends do not hold in wastewater.

Photochemistry. PPRI steady-state concentrations vary from $(0.43{-}12.6) \times 10^{-13}$ and $(0.57{-}32.5) \times 10^{-15}$ M for $[^1O_2]_{ss}$ and $[{}^\bullet OH]_{ss}$, respectively (Table S9). Generally, steady-state concentrations of both PPRI increase with increasing [DOC]. Quantum yields range from $(0.6{-}8.27) \times 10^{-2}$ (average = 3.5×10^{-2}) and $(0.34{-}105) \times 10^{-5}$ (average = 15×10^{-5}) for $^1O_2$ and ${}^\bullet OH$, respectively, while f_{TMP} ranges from 11.6 to 87.1 M^{-1} (average = 36.2 M^{-1}; Table S10). These values are within ranges observed previously.[15,50,72] The two order of magnitude $\Phi_{{}^\bullet OH}$ range agrees with compilations of quantum yields from large data sets, with the exception of two samples taken from the same WWTP which are especially photoreactive with regard to ${}^\bullet OH$.[50] Relatively narrow ranges of quantum yields are observed by the geographical group with the exception of Twin Cities and wastewater samples (Figure 1). Note that nitrate photolysis is negligible under these conditions (Section S6).

Although photoreactivity is correlated with select measurements of bulk DOM composition, some relationships are consistent across the entire data set, while others are only observed in some types of waters. For example, f_{TMP} shows a positive relationship to $E_2{:}E_3$ across the entire data set (Figure

S26b, $p = 0.002$), while no universal relationships are observed for f_{TMP} and $SUVA_{254}$, HIX, or FI (Figure S26; $p = 0.89$, 0.82, and 0.5, respectively). However, a positive relationship is observed between f_{TMP} and FI if only natural waters are considered (Figure S26d; $p = 0.01$). As observed with f_{TMP}, there is a positive relationship between $\Phi_{^1O_2}$ and $E_2{:}E_3$ in the full data set (Figure S27b; $p = 0.002$) but no relationship with $SUVA_{254}$ (Figure S27a; $p = 0.08$) or HIX (Figure S27c; $p = 0.34$). Additionally, there is a positive relationship with FI across the entire data set (Figure S27d; $p = 0.008$). In agreement with other studies,[14,31] $\Phi_{{}^\bullet OH}$ is not strongly related to $SUVA_{254}$, HIX, or FI (Figure S28; $p = 0.89$, 0.62, and 0.06, respectively). The weak negative relationship between $\Phi_{{}^\bullet OH}$ and $E_2{:}E_3$ ($p = 0.009$) is driven by several wastewater samples that have low values of $E_2{:}E_3$ but were highly photoreactive (Figure S28b). In summary, the strong relationships between f_{TMP} or $\Phi_{^1O_2}$ and $E_2{:}E_3$ observed in this large data set agree with observations made in previous studies.[14,16,31,73,74] The weaker relationships with $\Phi_{{}^\bullet OH}$ and optical properties also support previous observations of conflicting trends (e.g., both positive and negative relationships with $E_2{:}E_3$).[14,24] Similarly, conflicting correlations can be generated using the data in this study if only a subset of samples are considered. Therefore, past observations are likely attributable to small sample sizes typically used in photochemical studies.

EDC is closely associated with phenolic moieties within DOM.[23,65,66] Phenols have been implicated in other redox reactions including quenching of triplet radical cations and photochemical reduction of O_2 to form superoxide.[23] Thus, we hypothesized that EDC would be a strong predictor of photoreactivity. Here, we observe a negative relationship between EDC and $\Phi_{^1O_2}$ (Figure S29; $p = 0.02$) but no relationship to f_{TMP} or $\Phi_{{}^\bullet OH}$ ($p = 0.25$ and 0.23, respectively). Samples with higher EDC may have lower f_{TMP} and $\Phi_{^1O_2}$ due to low quantum yields for intersystem crossing from ^1DOM to ^3DOM as redox capacity can quench triplet states. However, the fact that ${}^\bullet OH$, which is hypothesized to form through redox reactions, does not show any relationship to EDC, means that other mechanisms or controlling factors must be considered. For example, it is possible that only a subset of molecules associated with high EDC form ${}^\bullet OH$ given the low $\Phi_{{}^\bullet OH}$ relative to other PPRI quantum yields. This lack of universal relationship between EDC and $\Phi_{{}^\bullet OH}$ refutes our hypothesis that EDC can be used as a bulk DOM composition parameter to predict $\Phi_{{}^\bullet OH}$ in natural waters.

As observed previously,[14] f_{TMP} and $\Phi_{^1O_2}$ are positively correlated across the entire data set (Figure S30a; $p = 1.1 \times 10^{-6}$). $\Phi_{{}^\bullet OH}$ is not related to f_{TMP} and weakly related to $\Phi_{^1O_2}$ (Figure S30; $p = 0.23$ and 0.09, respectively). This result demonstrates that unrelated pools of DOM are correlated to ^3DOM and $^1O_2$ versus ${}^\bullet OH$.

Relationships between quantum yields and DOM molecular composition provide insights into why many bulk properties are not correlated to quantum yields across the entire data set. Relationships between relative formula intensity and quantum yields fall in distinct areas of van Krevelen plots, but patterns depend on the geographical region considered (Figures S31−S33). Generally, saturated formulas are positively correlated to ^3DOM and $^1O_2$, which is consistent with previous observations.[14,16,26] There are some exceptions, including f_{TMP} in the SLR and correlations for the Mankato and Yahara samples.
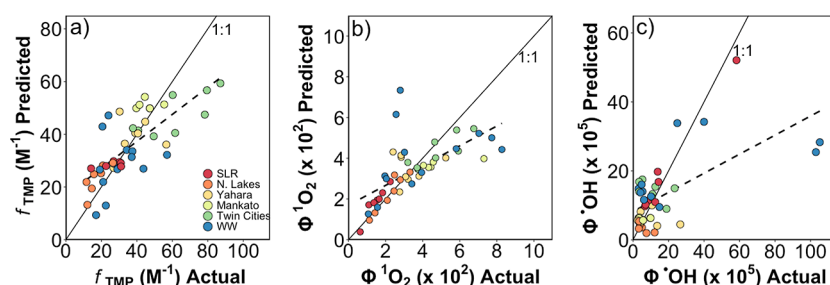
Figure 4. Results of MLR models for (a) f_{TMP}, (b) $\Phi_{^1O_2}$, and (c) $\Phi_{^•OH}$. Dashed lines represent the model results, while the solid lines represent 1:1 ratio.

The unexpected pattern of correlations for Yahara and Mankato sites may arise from the unique group of highly unsaturated formulas in these samples (Figure 3c,d). Alternatively, correlations may not be as robust in these groups due to their limited molecular ranges (Figure 2d,f). The lack of clustered correlations in wastewater samples is intriguing but not dissimilar to the lack of discernible correlations to EDC (Figure 3e,f). For $\Phi_{^•OH}$, formulas with lower H:C are more often positively correlated to quantum yields (Figure S33), in agreement with past observations in the SLR.[14]

Relationships between pools of DOM correlated to each PPRI formation are compared using Spearman rank rho values for natural and wastewater groups (Figure S34). The significant positive relationship between molecular-level correlations for $\Phi_{^1O_2}$ and f_{TMP} demonstrates the highly overlapping pools of DOM correlated to these PPRI (Figure S34a) in four of the six sample sets. The lack of a clear relationship is attributable to limited molecular diversity in the Yahara sites, and the small number of formulas negatively correlated with f_{TMP} in the SLR samples (Figure S32), as discussed above. Overall, these results clearly demonstrate that ^{3}DOM and $^1O_2$ are strongly related as expected given the $^1O_2$ formation mechanism. These trends have been observed in smaller data sets at the bulk[24,74] and molecular levels[14,16,73] but never tested in a large set of diverse waters. In contrast, even at the molecular level, there are no consistent relationships between $\Phi_{^•OH}$ and both $\Phi_{^1O_2}$ and f_{TMP}.

Multiple Linear Regressions. Because no single parameter shows strong correlations to all PPRI, MLR models are built for each quantum yield measured in this study using pH, $[NO_3^-]$, [Fe], [DIC], $SUVA_{254}$, E_2:E_3, HIX, FI, EDC, H:C_w, and O:C_w as potential predictor variables. These parameters are considered because both DOM composition and water chemistry can affect photochemical reactivity. For example, inorganic carbon species can quench $^•OH$.[55] Furthermore, nitrate and iron can both contribute to $^•OH$ production,[75,76] although nitrate photolysis is negligible under our irradiation conditions (Section S6).

The preferred model for f_{TMP} includes positive terms for [DIC], E_2:E_3, and HIX and a negative term for EDC (Figure 4; Table S11). The model for $\Phi_{^1O_2}$ includes positive terms for [DIC], E_2:E_3, and FI and negative terms for [Fe] and EDC (Table S12). Both models for f_{TMP} and $\Phi_{^1O_2}$ have positive terms for E_2:E_3 and negative terms for EDC, further demonstrating the close relationship of these PPRI. The observation that [DIC] and/or iron contribute to f_{TMP} and $\Phi_{^1O_2}$ is unexpected based on the known formation pathways of

these PPRI. The strength of these correlations is weaker than DOM-derived parameters, and they are likely present in the model because they describe surrounding land cover. For example, only rural samples have detectable amounts of iron, and these generally have lower $\Phi_{^1O_2}$ (Figures 1; S8).

The preferred model for $\Phi_{^•OH}$ includes positive terms for iron and FI, along with negative terms for O:C_w. It is unlikely that iron contributes to $^•OH$ in Fenton-like reactions under these conditions given the irradiation wavelengths and circumneutral pH. Rather, this term is attributable to the relatively high $\Phi_{^•OH}$ of rural samples. None of the parameters are included in all the models. The model for $\Phi_{^•OH}$ performs notably worse than the models for f_{TMP} or $\Phi_{^1O_2}$ ($p = 1.1 \times 10^{-4}$ for $\Phi_{^•OH}$ compared to 2.12×10^{-7} and 1.50×10^{-8} for $\Phi_{^1O_2}$ and f_{TMP}, respectively).

Overall, employment of these models results in stronger predictive power than any bulk or MS property alone, but the model for $\Phi_{^•OH}$ remains less accurate than f_{TMP} or $\Phi_{^1O_2}$ (Figure 4). All types of parameters (e.g., water chemistry, spectroscopic, fluorescence, EDC, and mass spectrometry) are included in some combination in the MLRs. This finding emphasizes that methods used to assess DOM composition are selective and only capture a fraction of this complex material, as observed previously.[58,77] For example, fluorescence spectroscopy only assesses the fraction of DOM that fluoresces, while FT-ICR MS only detects DOM that is retained by SPE and is amenable to the selected ionization technique. Furthermore, the inclusion of FT-ICR MS parameters limits the practicality of using these MLRs on a broad scale because these measurements are not easily accessible and may vary among laboratories.[78] However, their significance in the MLRs confirms that the DOM molecular composition determines its reactivity. Similarly, the inclusion of water chemistry parameters (e.g., NO_3^- and iron) points to land cover influences, which may vary in different regions. Nevertheless, the coefficients for DOM-related parameters are larger compared to inorganic species in all MLRs, demonstrating that the DOM composition is the key driver.

Environmental Significance. EDC is essential to understanding processes involving DOM. EDC has important implications in drinking water applications as it changes during disinfection and is related to formation of chlorinated disinfection byproducts and ozone reactivity.[11,45] The direct relationships drawn between EDC and DOM molecular composition in this study show that EDC is predominantly determined by the DOM composition in natural freshwaters and that tannin- and lignin-like compounds give rise to this redox activity, corroborating past measurements using humic

substance isolates.[65] In contrast, EDC in wastewater effluents is related to $SUVA_{254}$ but not clearly related to the DOM molecular composition. This could be evidence of a non-phenol donor group within DOM or potential interference from inorganic species in wastewater.

This large data set demonstrates that ^3DOM and $^1O_2$ are inherently related, as expected based on their formation mechanisms. In addition to strong correlations between f_{TMP} and $\Phi_{^1O_2}$, these parameters are related to the same bulk parameters (Figures S26, S27), associated with the same pool of DOM molecules (Figures S31, S32), and have similar MLR models (Tables S11, S12). Given the diversity of DOM samples in this study, the relationship between these PPRI is expected to be universal in freshwaters.

Whether or not ^3DOM is a precursor for $^\bullet OH$ remains up for debate. $^\bullet OH$ is important because of its fast and non-selective reactivity with many organic contaminants, including pesticides and pharmaceuticals.[79,80] Additionally, the wide-spread practice of using ^3DOM quenchers such as sorbic acid and comparison of results in anoxic versus oxic conditions to differentiate between ^3DOM and $^1O_2$ may be overlooking potential effects of ^3DOM quenching on $^\bullet OH$.[14,15,81] Thus, incomplete understanding of $^\bullet OH$ formation mechanisms also results in incomplete understanding of contaminant transformation pathways.

The results of this study demonstrate that the ability to accurately predict $\Phi_{^\bullet OH}$ is lacking compared to other PPRI like ^3DOM and $^1O_2$. Compositional parameters derived from spectroscopy and mass spectrometry data hold predictive power in some subsets of our samples but are largely incapable of describing $\Phi_{^\bullet OH}$ across the entire data set. Surprisingly, EDC is not successful at predicting $\Phi_{^\bullet OH}$ although it is negatively related to $\Phi_{^1O_2}$, likely because redox active moieties quench ^3DOM.[82] $\Phi_{^\bullet OH}$ is best predicted by the MLR model rather than simple linear regressions, but this approach still has much more error associated with it than models for f_{TMP} or $\Phi_{^1O_2}$. Thus, actual measurements of PPRI in whole water samples will likely remain necessary to confirm predicted photochemical transformation of organic contaminants.

ASSOCIATED CONTENT

Supporting Information

The Supporting Information is available free of charge at https://pubs.acs.org/doi/10.1021/acs.est.3c01157.

Additional experimental details, water chemistry parameters, and MLR outputs (PDF)

AUTHOR INFORMATION

Corresponding Author

Christina K. Remucal − *Environmental Chemistry and Technology Program and Department of Civil and Environmental Engineering, University of Wisconsin—Madison, Madison, Wisconsin 53706, United States;* orcid.org/0000-0003-4285-7638; Phone: (608) 262-1820; Email: remucal@wisc.edu; Fax: (608) 262-0454

Authors

Stephanie M. Berg − *Environmental Chemistry and Technology Program, University of Wisconsin—Madison, Madison, Wisconsin 53706, United States;* orcid.org/0000-0001-5971-6124

Kristine H. Wammer − *Department of Chemistry, University of St. Thomas, St. Paul, Minnesota 55105, United States;* orcid.org/0000-0003-2067-892X

Complete contact information is available at:
https://pubs.acs.org/10.1021/acs.est.3c01157

Notes

The authors declare no competing financial interest.

REFERENCES

(1) Cole, J. J.; Prairie, Y. T.; Caraco, N. F.; McDowell, W. H.; Tranvik, L. J.; Striegl, R. G.; Duarte, C. M.; Kortelainen, P.; Downing, J. A.; Middelburg, J. J.; Melack, J. Plumbing the global carbon cycle: Integrating inland waters into the terrestrial carbon budget. *Ecosystems* **2007**, *10*, 172−185.

(2) Brown, A.; McKnight, D. M.; Chin, Y. P.; Roberts, E. C.; Uhle, M. Chemical characterization of dissolved organic material in Pony Lake, a saline coastal pond in Antarctica. *Mar. Chem.* **2004**, *89*, 327−337.

(3) Gonsior, M.; Peake, B. M.; Cooper, W. T.; Podgorski, D.; D'Andrilli, J.; Cooper, W. J. Photochemically induced changes in dissolved organic matter identified by ultrahigh resolution Fourier transform ion cyclotron resonance mass spectrometry. *Environ. Sci. Technol.* **2009**, *43*, 698−703.

(4) Wasswa, J.; Driscoll, C. T.; Zeng, T. Contrasting impacts of photochemical and microbial processing on the photoreactivity of dissolved organic matter in an Adirondack Lake watershed. *Environ. Sci. Technol.* **2022**, *56*, 1688−1701.

(5) Ward, C. P.; Nalven, S. G.; Crump, B. C.; Kling, G. W.; Cory, R. M. Photochemical alteration of organic carbon draining permafrost soils shifts microbial metabolic pathways and stimultes respiration. *Nat. Commun.* **2017**, *8*, 1−7.

(6) Raeke, J.; Lechtenfeld, O. J.; Seiwert, B.; Meier, T.; Riemenschneider, C.; Reemtsma, T. Photochemically induced bound residue formation of carbamazepine with dissolved organic matter. *Environ. Sci. Technol.* **2017**, *51*, 5523−5530.

(7) Remucal, C. K. The role of indirect photochemical degradation in the environmental fate of pesticides: A review. *Environ. Sci.: Processes Impacts* **2014**, *16*, 628−653.

(8) Boreen, A. L.; Arnold, W. A.; McNeill, K. Photodegradation of pharmaceuticals in the aquatic environment: A review. *Aquat. Sci.* **2003**, *65*, 320−341.

(9) Barazesh, J. M.; Prasse, C.; Wenk, J.; Berg, S.; Remucal, C. K.; Sedlak, D. L. Trace element removal in distributed drinking water treatment systems by cathodic H_2O_2 production and UV photolysis. *Environ. Sci. Technol.* **2018**, *52*, 195−204.

(10) Bulman, D. M.; Remucal, K. Role of reactive halogen species in disinfection byproduct formation during chlorine photolysis. *Environ. Sci. Technol.* **2020**, *54*, 9629−9639.

(11) Remucal, C. K.; Salhi, E.; Walpen, N.; von Gunten, U. Molecular-level transformation of dissolved organic matter during

oxidation by ozone and hydroxyl radical. *Environ. Sci. Technol.* **2020**, *54*, 10351−10360.

(12) Green, S. A.; Blough, N. V. Optical absorption and fluorescence properties of chromophoric dissolved organic matter in natural waters. *Limnol. Oceanogr.* **1994**, *39*, 1903−1916.

(13) McNeill, K.; Canonica, S. Triplet state dissolved organic matter in aquatic photochemistry: Reaction mechanisms, substrate scope, and photophysical properties. *Environ. Sci.: Processes Impacts* **2016**, *18*, 1381−1399.

(14) Berg, S. M.; Whiting, Q. T.; Herrli, J. A.; Winkels, R.; Wammer, K. H.; Remucal, C. K. The role of dissolved organic matter composition in determining photochemical reactivity at the molecular level. *Environ. Sci. Technol.* **2019**, *53*, 11725−11734.

(15) Zeng, T.; Arnold, W. A. Pesticide photolysis in prairie potholes: Probing photosensitized processes. *Environ. Sci. Technol.* **2013**, *47*, 6735−6745.

(16) Maizel, A. C.; Li, J.; Remucal, C. K. Relationships between dissolved organic matter composition and photochemistry in lakes of diverse trophic status. *Environ. Sci. Technol.* **2017**, *51*, 9624−9632.

(17) Sardana, A.; Weaver, L.; Aziz, T. N. Effects of dissolved organic matter characteristics on the photosensitized degradation of pharmaceuticals in wastewater treatment wetlands. *Environ. Sci.: Processes Impacts* **2022**, *24*, 805−824.

(18) Garg, S.; Rose, A. L.; Waite, T. D. Production of reactive oxygen species on photolysis of dilute aqueous quinone solutions. *Photochem. Photobiol.* **2007**, *83*, 904−913.

(19) Couch, K.; Leresche, F.; Farmer, C.; McKay, G.; Rosario-Ortiz, F. L. Assessing the source of the photochemical formation of hydroxylating species from dissolved organic matter using model sensitizers. *Environ. Sci.: Processes Impacts* **2022**, *24*, 102−115.

(20) Page, S. E.; Arnold, W. A.; McNeill, K. Assessing the contribution of free hydroxyl radical in organic matter-sensitized photohydroxylation reactions. *Environ. Sci. Technol.* **2011**, *45*, 2818−2825.

(21) Garg, S.; Rose, A. L.; Waite, T. D. Photochemical production of superoxide and hydrogen peroxide from natural organic matter. *Geochim. Cosmochim. Acta* **2011**, *75*, 4310−4320.

(22) McKay, G.; Couch, K. D.; Mezyk, S. P.; Rosario-Ortiz, F. L. Investigation of the coupled effects of molecular weight and charge-transfer interactions on the optical and photochemical properties of dissolved organic matter. *Environ. Sci. Technol.* **2016**, *50*, 8093−8102.

(23) Ma, J.; Nie, J.; Zhou, H.; Wang, H.; Lian, L.; Yan, S.; Song, W. Kinetic consideration of photochemical formation and decay of superoxide radical in dissolved organic matter solutions. *Environ. Sci. Technol.* **2020**, *54*, 3199−3208.

(24) McCabe, A. J.; Arnold, W. A. Seasonal and spatial variabilities in the water chemistry of prairie pothole wetlands influence the photoproduction of reactive intermediates. *Chemosphere* **2016**, *155*, 640−647.

(25) Bodhipaksha, L. C.; Sharpless, C. M.; Chin, Y. P.; Sander, M.; Langston, W. K.; Mackay, A. A. Triplet photochemistry of effluent and natural organic matter in whole water and isolates from effluent-receiving rivers. *Environ. Sci. Technol.* **2015**, *49*, 3453−3463.

(26) McCabe, A. J.; Arnold, W. A. Reactivity of triplet excited states of dissolved natural organic matter in stormflow from mixed-use watersheds. *Environ. Sci. Technol.* **2017**, *51*, 9718−9728.

(27) Mostafa, S.; Rosario-Ortiz, F. L. Singlet oxygen formation from wastewater organic matter. *Environ. Sci. Technol.* **2013**, *47*, 8179−8186.

(28) Peterson, B. M.; McNally, A. M.; Cory, R. M.; Thoemke, J. D.; Cotner, J. B.; McNeill, K. Spatial and temporal distribution of singlet oxygen in Lake Superior. *Environ. Sci. Technol.* **2012**, *46*, 7222−7229.

(29) Sharpless, C. M. Lifetimes of triplet dissolved natural organic matter (DOM) and the effect of $NaBH_4$ reduction on singlet oxygen quantum yields: Implications for DOM photophysics. *Environ. Sci. Technol.* **2012**, *46*, 4466−4473.

(30) Sharpless, C. M.; Aeschbacher, M.; Page, S. E.; Wenk, J.; Sander, M.; McNeill, K. Photooxidation-induced changes in optical,

electrochemical, and photochemical properties of humic substances. *Environ. Sci. Technol.* **2014**, *48*, 2688−2696.

(31) McKay, G.; Huang, W.; Romera-Castillo, C.; Crouch, J. E.; Rosario-Ortiz, F. L.; Jaffe, R. Predicting reactive intermediate quantum yields from dissolved organic matter photolysis using optical properties and antioxidant capacity. *Environ. Sci. Technol.* **2017**, *51*, 5404−5413.

(32) Dong, M. M.; Rosario-Ortiz, F. L. Photochemical formation of hydroxyl radical from effluent organic matter. *Environ. Sci. Technol.* **2012**, *46*, 3788−3794.

(33) Sharpless, C. M.; Blough, N. V. The importance of charge-transfer interactions in determining chromophoric dissolved organic matter (CDOM) optical and photochemical properties. *Environ. Sci.: Processes Impacts* **2014**, *16*, 654−671.

(34) Page, S. E.; Logan, J. R.; Cory, R. M.; McNeill, K. Evidence for dissolved organic matter as the primary source and sink of photochemically produced hydroxyl radical in Arctic surface waters. *Environ. Sci.: Processes Impacts* **2014**, *16*, 807−822.

(35) Glover, C. M.; Rosario-Ortiz, F. L. Impact of halides on the photoproduction of reactive intermediates from organic matter. *Environ. Sci. Technol.* **2013**, *47*, 13949−13956.

(36) Canonica, S.; Laubscher, H. U. Inhibitory effect of dissolved organic matter on triplet-induced oxidation of aquatic contaminants. *Photochem. Photobiol. Sci.* **2008**, *7*, 547−551.

(37) Chen, Y.; Hozalski, R. M.; Olmanson, L. G.; Page, B. P.; Finlay, J. C.; Brezonik, P.; Arnold, A. Prediction of photochemically produced reactive intermediates in surface waters via satellite remote sensing. *Environ. Sci. Technol.* **2020**, *54*, 6671−6681.

(38) Weishaar, J.; Aiken, G.; Bergamaschi, B.; Fram, M.; Fujii, R.; Mopper, K. Evaluation of specific ultra-violet absorbance as an indicator of the chemical content of dissolved organic carbon. *Environ. Sci. Technol.* **2003**, *37*, 4702−4708.

(39) Helms, J. R.; Stubbins, A.; Ritchie, J. D.; Minor, E. C.; Kieber, D. J.; Mopper, K. Absorption spectral slopes and slope ratios as indicators of molecular weight, source, and photobleaching of chromophoric dissolved organic matter. *Limnol. Oceanogr.* **2008**, *53*, 955−969.

(40) Peuravuori, J.; Pihlaja, K. Molecular size distribution and spectroscopic properties of aquatic humic substances. *Anal. Chim. Acta* **1997**, *337*, 133−149.

(41) Ohno, T. Fluorescence inner-filtering correction for determining the humification index of dissolved organic matter. *Environ. Sci. Technol.* **2002**, *36*, 742−746.

(42) Korak, J. A.; Dotson, A. D.; Summers, R. S.; Rosario-Ortiz, F. L. Critical analysis of commonly used fluorescence metrics to characterize dissolved organic matter. *Water Res.* **2014**, *49*, 327−338.

(43) Dittmar, T.; Koch, B.; Hertkorn, N.; Kattner, G. A simple and efficient method for the solid-phase extraction of dissolved organic matter (SPE-DOM) from seawater. *Limnol Oceanogr. Methods* **2008**, *6*, 230−235.

(44) Koch, B. P.; Dittmar, T.; Witt, M.; Kattner, G. Fundamentals of molecular formula assignment to ultrahigh resolution mass data of natural organic matter. *Anal. Chem.* **2007**, *79*, 1758−1763.

(45) Walpen, N.; Houska, J.; Salhi, E.; Sander, M.; von Gunten, U. Quantification of the electron donating capacity and UV absorbance of dissolved organic matter during ozonation of secondary wastewater effluent by an assay and an automated analyzer. *Water Res.* **2020**, *185*, 116235.

(46) Bulman, D. M.; Mezyk, S. P.; Remucal, C. K. The impact of pH and irradiation wavelength on the production of reactive oxidants during chlorine photolysis. *Environ. Sci. Technol.* **2019**, *53*, 4450−4459.

(47) Maizel, A. C.; Remucal, C. K. The effect of probe choice and solution conditions on the apparent photoreactivity of dissolved organic matter. *Environ. Sci.: Processes Impacts* **2017**, *19*, 1040−1050.

(48) Page, S. E.; Arnold, W. A.; McNeill, K. Terephthalate as a probe for photochemically generated hydroxyl radical. *J. Environ. Monit.* **2010**, *12*, 1658−1665.

(49) Appiani, E.; Ossola, R.; Latch, D. E.; Erickson, P. R.; McNeill, K. Aqueous singlet oxygen reaction kinetics of furfuryl alcohol: Effect of temperature, pH, and salt content. *Environ. Sci.: Processes Impacts* **2017**, *19*, 507−516.

(50) Wasswa, J.; Driscoll, C. T.; Zeng, T. Photochemical characterization of surface waters from lakes in the Adirondack region of New York. *Environ. Sci. Technol.* **2020**, *54*, 10654−10667.

(51) Laszakovits, J. R.; Berg, S. M.; Anderson, B. G.; O'Brien, J. E.; Wammer, K. H.; Sharpless, C. M. *p*-Nitroanisole/pyridine and *p*-nitroacetophenone/pyridine actinometers revisited: Quantum yield in comparison to ferrioxalate. *Environ. Sci. Technol. Lett.* **2017**, *4*, 11−14.

(52) Milstead, R. P.; Remucal, C. K. Molecular-level insights into the formation of traditional and novel halogenated disinfection by-products. *ACS ES&T Water* **2021**, *1*, 1966−1974.

(53) Berg, S. M.; Peterson, B. D.; McMahon, K. D.; Remucal, C. K. Spatial and temporal variability of dissolved organic matter molecular composition in a stratified eutrophic lake. *J. Geophys. Res.: Biogeosci.* **2022**, *127*, 1−16.

(54) Parker, K. M.; Pignatello, J. J.; Mitch, W. A. Influence of ionic strength on triplet-state natural organic matter loss by energy transfer and electron transfer pathways. *Environ. Sci. Technol.* **2013**, *47*, 10987−10994.

(55) Jasper, J. T.; Sedlak, D. L. Phototransformation of wastewater-derived trace organic contaminants in open-water unit process treatment wetlands. *Environ. Sci. Technol.* **2013**, *47*, 10781−10790.

(56) Berg, S. M.; Mooney, R. J.; McConville, M. B.; McIntyre, P. B.; Remucal, C. K. Seasonal and spatial variability of dissolved carbon concentration and composition in Lake Michigan tributaries. *J. Geophys. Res.: Biogeosci.* **2021**, *126*, 1−14.

(57) Southworth, B. A.; Voelker, B. M. Hydroxyl radical production via the photo-fenton reaction in the presence of fulvic acid. *Environ. Sci. Technol.* **2003**, *37*, 1130−1136.

(58) Maizel, A. C.; Remucal, C. K. The effect of advanced secondary municipal wastewater treatment on the molecular composition of dissolved organic matter. *Water Res.* **2017**, *122*, 42−52.

(59) Gonsior, M.; Zwartjes, M.; Cooper, W. J.; Song, W.; Ishida, K. P.; Tseng, L. Y.; Jeung, M. K.; Rosso, D.; Hertkorn, N.; Schmitt-Kopplin, P. Molecular characterization of effluent organic matter identified by ultrahigh resolution mass spectrometry. *Water Res.* **2011**, *45*, 2943−2953.

(60) Coble, P. G. Characterization of marine and terrestrial DOM in seawater using excitation-emission matrix spectroscopy. *Mar. Chem.* **1996**, *51*, 325−346.

(61) Lusk, M. G.; Toor, G. S. Dissolved organic nitrogen in urban streams: Biodegradability and molecular composition studies. *Water Res.* **2016**, *96*, 225−235.

(62) Zhou, Y.; Cheng, F.; He, D.; Zhang, Y.; Qu, J.; Yang, X.; Chen, J.; Peijnenburg, W. J. G. M. Effect of UV/chlorine treatment on photophysical and photochemical properties of dissolved organic matter. *Water Res.* **2021**, *192*, 116857.

(63) Önnby, L.; Walpen, N.; Salhi, E.; Sander, M.; von Gunten, U. Two analytical approaches quantifying the electron donating capacities of dissolved organic matter to monitor Its oxidation during chlorination and ozonation. *Water Res.* **2018**, *144*, 677−689.

(64) Wu, Q. Y.; Zhou, T. H.; Du, Y.; Ye, B.; Wang, W. L.; Hu, H. Y. Characterizing the molecular weight distribution of dissolved organic matter by measuring the contents of electron-donating moieties, UV absorbance, and fluorescence intensity. *Environ. Int.* **2020**, *137*, 105570.

(65) Aeschbacher, M.; Graf, C.; Schwarzenbach, R. P.; Sander, M. Antioxidant properties of humic substances. *Environ. Sci. Technol.* **2012**, *46*, 4916−4925.

(66) Walpen, N.; Schroth, M. H.; Sander, M. Quantification of phenolic antioxidant moieties in dissolved organic matter by flow-injection analysis with electrochemical detection. *Environ. Sci. Technol.* **2016**, *50*, 6423−6432.

(67) Nurmi, J. T.; Tratnyek, P. G. Electrochemical properties of natural organic matter (NOM), fractions of NOM, and model

biogeochemical electron shuttles. *Environ. Sci. Technol.* **2002**, *36*, 617−624.

(68) Ratasuk, N.; Nanny, M. A. Characterization and quantification of reversible redox sites in humic substances. *Environ. Sci. Technol.* **2007**, *41*, 7844−7850.

(69) Yang, P.; Jiang, T.; Cong, Z.; Liu, G.; Guo, Y.; Liu, Y.; Shi, J.; Hu, L.; Yin, Y.; Cai, Y.; Jiang, G. Loss and increase of the electron exchange capacity of natural organic matter during its reduction and reoxidation: The role of quinone and nonquinone moieties. *Environ. Sci. Technol.* **2022**, *56*, 6744−6753.

(70) Aeschbacher, M.; Sander, M.; Schwarzenbach, R. P. Novel electrochemical approach to assess the redox properties of humic substances. *Environ. Sci. Technol.* **2010**, *44*, 87−93.

(71) Fimmen, R. L.; Cory, R. M.; Chin, Y. P.; Trouts, T. D.; McKnight, D. M. Probing the oxidation-reduction properties of terrestrially and microbially derived dissolved organic matter. *Geochim. Cosmochim. Acta* **2007**, *71*, 3003−3015.

(72) Ossola, R.; Jönsson, O. M.; Moor, K.; McNeill, K. Singlet oxygen quantum yields in environmental waters. *Chem. Rev.* **2021**, *121*, 4100−4146.

(73) Maizel, A. C.; Remucal, C. K. Molecular composition and photochemical reactivity of size-fractionated dissolved organic matter. *Environ. Sci. Technol.* **2017**, *51*, 2113−2123.

(74) Dalrymple, R. M.; Carfagno, A. K.; Sharpless, C. M. Correlations between dissolved organic matter optical properties and quantum yields of singlet oxygen and hydrogen peroxide. *Environ. Sci. Technol.* **2010**, *44*, 5824−5829.

(75) Vermilyea, A. W.; Voelker, B. M. Photo-fenton reaction at near neutral pH. *Environ. Sci. Technol.* **2009**, *43*, 6927−6933.

(76) Benedict, K. B.; McFall, A. S.; Anastasio, C. Quantum yield of nitrite from the photolysis of aqueous nitrate above 300 nm. *Environ. Sci. Technol.* **2017**, *51*, 4387−4395.

(77) Hawkes, J. A.; Sjöberg, P. J. R.; Bergquist, J.; Tranvik, L. J. Complexity of cissolved organic matter in the molecular size dimension: Insights from coupled size exclusion chromatography electrospray ionisation mass spectrometry. *Faraday Discuss.* **2019**, *218*, 52−71.

(78) Hawkes, J. A.; D'Andrilli, J.; Agar, J. N.; Barrow, M. P.; Berg, S. M.; Catalán, N.; Chen, H.; Chu, R. K.; Cole, R. B.; Dittmar, T.; Gavard, R.; Gleixner, G.; Hatcher, P. G.; He, C.; Hess, N. J.; Hutchins, R. H. S.; Ijaz, A.; Jones, H. E.; Kew, W.; Khaksari, M.; Palacio Lozano, D. C.; Lv, J.; Mazzoleni, L. R.; Noriega-Ortega, B. E.; Osterholz, H.; Radoman, N.; Remucal, C. K.; Schmitt, N. D.; Schum, S. K.; Shi, Q.; Simon, C.; Singer, G.; Sleighter, R. L.; Stubbins, A.; Thomas, M. J.; Tolic, N.; Zhang, S.; Zito, P.; Podgorski, D. C. An international laboratory comparison of dissolved organic matter composition by high resolution mass spectrometry: Are we getting the same answer? *Limnol Oceanogr. Methods* **2020**, *18*, 235−258.

(79) Lian, L.; Yao, B.; Hou, S.; Fang, J.; Yan, S.; Song, W. Kinetic study of hydroxyl and sulfate radical-mediated oxidation of pharmaceuticals in wastewater effluents. *Environ. Sci. Technol.* **2017**, *51*, 2954−2962.

(80) Buxton, G. V.; Greenstock, C. L.; Helman, W. P.; Ross, A. B. Critical review of rate constants for reactions of hydrated electrons, hydrogen atoms, and hydroxyl radical (OH/O⁻) in aqueous solutions. *J. Phys. Chem. Ref. Data* **1988**, *17*, 513−886.

(81) McConville, M. B.; Mezyk, S. P.; Remucal, C. K. Indirect photodegradation of the lampricides TFM and niclosamide. *Environ. Sci.: Processes Impacts* **2017**, *19*, 1028−1039.

(82) McKay, G. Emerging investigator series: Critical review of photophysical models for the optical and photochemical properties of dissolved organic matter. *Environ. Sci.: Processes Impacts* **2020**, *22*, 1139−1165.

(83) Laszakovits, J. R.; MacKay, A. A. Data-based chemical class regions for van Krevelen diagrams. *J. Am. Soc. Mass Spectrom.* **2022**, *33*, 198−202.